韓國非破壞檢査 第3卷 第2號, pp. 13～27, 1983

《技術報告》

두꺼운 바이메탈 熔接에 대한 超音波 探傷方法의 改善

Contribution to Improving Ultrasonic Testing of Thick Bimetallic Welds

DANIEL MONTALT – RENE BARBIER
FRAMATOME-EXPORT (FRAMEX), KOREA BRANCH

1. INTRODUCTION.

The need for safety of nuclear power installations is forcing engineers to find ways and means of efficiently testing austanitic weld joints.

In view of the advantages of ultrasonic testing, which is used with success for ferritic weld joints, development of more effective methods for austenitic weld inspection is an important objective in the nuclear industry.

FRAMATOME is cooperating with WESTINGHOUSE, ELECTRICITE DE FRANCE and the COMMISARIAT A L'ENERGIE ATOMIQUE to determine the capabilities and reliability of ultrasonic testing procedures for detecting flaws in austenitic steels and bimetallic weldments.

A particular section of FRAMATOME'S work, performed at the INSA Laboratory in Lyon, is concerned with the study of thick bimetallic welds between forged and cast stainless and ferritic steels.

Ultrasonic testing of such weldments is complicated by the phenomenon of "anisotropic scattering" which produces considerable back-ground noise, spurious echoes and an isotropic attenuation of ultrasonic waves.

An analytical study of the ultrasonic wave propagation in the various areas of two kinds of thick bimetallic welds anables us to determine the characteristics of special probes which will be tested on artificial and actual flaws.

2. METALLURGY.

2.1. Description of the two bimetallic joints.

2.1.1. Weldment (I) between forged ferritic and forged austenitic steels.

This weldment is composed of 5 areas (Fig. 1):

(A) forged ferritic low carbon steel (SA 508 C1. 3),

(B) buttering composed of 24 Cr – 12 Ni stainless steel for the first layer and 20 Cr – 10 Ni – 3 Mo for the other layers, applied with a covered electrode,

(C) homogeneous weld composed of 20 Cr – 10 Ni – 3 Mo stainless steel, applied with a covered electrode,

(D) forged austenitic stainless steel (Z 3 CND 17-12),

(E) cladding composed of 24 Cr – 12 Ni stainless steel for the first layer and 20 Cr – 10 Ni – 3 Mo for the other two layers, applied using automatic technique.

2.1.2. Weldment (II) between cast ferritic and cast austenitic steels.

This weldment is also composed of 5 areas (Fig. 2):

(A) cast ferritic low carbon steel (SA 216 grade WCC),

(B) buttering with the same composition as 2.1.1. (B),

(C) homogeneous weld with the same composition as 2.1.1. (C),

(D) cast austenitic stainless steel (Z3 CND 17-12),

(E) cladding with the same composition as 2.1.1. (E) but applied with a covered electrode.

2.2. Metallographic study.

2.2.1. Weldment (I) (Fig. I).

(A) forged ferritic steel:

micrographic examination (m.e) revealed a very fine grained ferrite and cementite texture (the grain size according to AFNOR A04. 102 is G = 11).

(B) buttering:

macrographic examination (M.E) revealed the edges of the successive weld runs and unidirectional crystallization perpendicular to the weld preparation and to these runs. The grains follow the heat paths in the weld during cooling and they often grow epitaxially from one weld run to another. The grains are columnar in shape; they are about 1 mm wide and up to several centimeters long.

m.c. revealed:

– in a plane perpendicular to the weld axis, a ferrite lattice (7%) marking the limits of austenitic matrix crystallization. Important variations in the lattice shape occur between two weld runs,

– in a plane parallel to the weld axis, a regular ferrite lattice without any special direction.

(C) homogeneous weld:

M.E. revealed variable crystallization around a principal axis coinciding with the axis of symmetry of the preparation. The dendritic texture has the same characteristics as in 2.2.1 (B).

(D) forged austenitic stainless steel:

m.e. revealed a classical austenitic twinned texture (G = 3 to 4).

(E) cladding:

The dendritic texture has the same characteristics as in 2.2.1 (B).

2.2.2. Weldment (II) (Fig. 2).

(A) cast ferritic steel:

m.e. revealed a very fine-grained ferrite and lamellar perlite texture (G = 10),

(B) buttering: same texture as in 2.2.1 (B),

(C) homogeneous weld: same texture as in 2.2.1 (C),

(D) cast austenoferritic stainless steel:

M.E. revealed a coarse texture with streaked grains. These grains are equiaxial on the edge (grain size $\simeq$ 3mm); but in central area, the grains increase to 4mm x 10mm in size and are perpendicular to the weld axis.

m.e. revealed a coarse texture with a thick ferrite lattice (30%),

(E) cladding: same texture as in 2.2.1 (E).

3. ULTRASONIC WAVE PROPAGATION

3.1. Measurement methods.

Cylindrical samples (19.4 or 35.3mm in diameter) were taken from the various areas of each weldment parallel to its axis.

The study of ultrasonic longitudinal wave propagation (attenuation and velocity) was performed using the apparatus shown in Fig. 3: the cylindrical samples were placed between transmitting and receiving transducers (two Panametrics V115, ϕ 0.75', 10 MHz broadband with plexiglass lenses) so that the beam passed through the diameter of the specimen. The ultrasonic longitudinal beam propagation characteristics of the samples were studied by rotating them in the beam.

3.1.1. Attenuation measurements.

Owing to the choice of tuning of Panametrics 5052 PR pulser-receiver and Hewlett Packard 141 T Spectrum Analyser, a constant frequency spectrum level was obtained on ferritic samples for frequency between 1 and 5 MHz. This level was considered as the reference level. For anisotropic samples, attenuation was plotted against this level for angles increasing 5° at a time.

3.1.2. Velocity measurements.

Only velocity curves were plotted for non interface cylindrical samples. Velocity and attenuation measurements were obtained from the same screen displays.

3.2. Results.

3.2.1. Ultrasonic longitudinal wave propagation in the various areas of weldment (I).

3.2.1.1. Ferritic forged steel.

- Attenuation: isotropic. A constant level of between 1 and 5 MHz was considered as reference.
- Velocity: constant at 5950 m/s.

3.2.1.2. Austenitic forged stainless steel.

- Relative attenuation: isotropic. Relative attenuation was negligable for low frequencies (1 MHz) but increased in upper frequency ranges. We found a relative attenuation coefficient α ie.
  α [dB/cm] = 0.04 f^2 [MHz] with 3 MHz $\leqslant f \leqslant$ 5 MHz.
- Velocity was constant at 5790m/s.

3.2.1.3. Dendritic areas (buttering and homogeneous weld).

- Relative attenuation was anisotropic and the variations of attenuation observed was markedly cyclic, having a period of 90°.
  Attenuation was weaker at low frequencies and the gap between maximum and minimum decreased at lower frequencies. These extremes remained unaltered when frequency was varied.
  The axis of least attenuation was regularly observed at an angle of 45° to the grain alignment axis of the dendritic texture. A specimen curve is given in Fig. 4.
  It seems that attenuation in this kind of dendritic texture was caused by curvature of the incident beam as
  1) only slight variations in background noise was observed when sample was rotated;
  2) in an angular position with transmitted signal reduced to minimum, a stronger signal was obtained when a 2mm receiving transducer was displaced perpendicularly with respect to the incident ultrasonic beam.
- Velocity was anisotropic, the variation was cyclic with a period of 90°. In the homogeneous weld (Fig. 5), the maximum velocity was 6,120m/s and the minimum 5,250 m/s (difference of 15%).

In the buttering, the maximum velocity was 6,280m/s and the minimum 5,270m/s (difference of 16%).

The maximum velocity corresponds to the maximum attenuation. However, it should be noted that these measurements only indicate "apparent" attenuation and velocity in the incident ultrasonic beam direction owing to beam curvature phenomenon.

3.2.1.4. Global attenuation.

In Fig. 6, attenuation was plotted as a function of angular position for each cylindrical sample. For a given scanning surface, the direction of least attenuation corresponds to the minimum when attenuation curves for cylindrical samples representing the various areas through which ultrasonic waves pass to reach a given point in the weld are superimposed.

3.2.2. Ultrasonic longitudinal wave propagation in the various areas of weldment (II).

3.2.2.1. Ferritic cast steel and dendritic areas.

– Attenuation and velocity: same results as in 3.2.1.1. and 3.2.1.3.

3.2.2.2. Austenoferritic cast stainless steel.

Variations were small enough to enable the sample to be considered as isotropic for attenuation and velocity.

– Attenuation was slight at 1MHz but greatly increased at higher frequencies ie α [dB/cm] = 0.7 f [MHz] with 2 MHz $\leqslant$ f $\leqslant$ 5 MHz.

3.2.2.3. Global attenuation.

In Fig. 7, we plotted attenuation as a function of angular position for each cylindrical sample.

4. OPTIMIZATION OF DETECTION OF ARTIFICIAL REFLECTORS.

Various artificial reflectors (3mm diameter side drilled holes and 3 x 3mm notches) are machined in 50mm wide test-blocks representative of each weldment (Fig. 8).

The tests were performed under water with following variables: wave mode, refraction angle in steel and frequency.

To detect reflectors, several factors were taken into consideration: the crossing of the water/steel interface, attenuation particular to each material for a given angle of incidence, the crossing of interfaces between steels if it occurs, and variation in the path of ultrasounds according to the angle of incidence.

4.1. The effect of wave mode.

The tests performed with longitudinal waves gave better results than with transverse waves at same frequency or wavelength.

4.2. The effect of refraction angle in steel.

Each reflector was examined from both surfaces for refracted angles in steel increasing in 10° steps. We used a CGR Ultrasonic R7 flaw detector and a Panametrics V 305 (0. 75" in diameter – 2.25 MHz) transducer. The reference amplification (OdB) was obtained for an amplitude signal 6/7 the height of the screen on a 2mm diameter side drilled hole machined at a depth of 50mm in a ferritic test-block possessing the same ultrasonic properties as the IIS block. At each measurement position, the amplification needed to produce an amplitude signal 6/7 the height of the screen, the apparent ultrasonic sound path and the signal to noise (S/N) ratio were plotted.

4.2.1. Weldment (I).

1) The two parent materials (ferritic forged steel and austenitic forged stainless steel) are very permeable to ultrasonic waves this permeability is not very different in these two materials. On the other hand, the dendritic textures of the buttering, the cladding and the homogeneous weld are very difficult to cross and induced phenomena such as: high degree of anisotropic attenuation, very low signal to noise ratio, curvature of the ultrasonic beam and spurious echoes.

2) In each of the four possible scanning directions, all the reflectors were detected if the angle θ refracted in the steel is such that $40^\circ \leqslant \theta \leqslant 50^\circ$, as already noted in Fig. 6.

3) The mean difference in amplitude for echoes associated with a line of reflectors at the same depth was generally smaller for $\theta \geqslant 40^\circ$.

4) Only $\theta = 45^\circ$ allowed a S/N ratio > 12 dB for all the reflectors and in the four scanning directions(an exception however: S/N 9 dB in the screen display for hole n°. 2 examined from the cladded surface through austenitic stainless steel parent material).

5) There were many structural spurious echoes at small refracted angles ($\theta \leqslant 30^\circ$) and angles close to weld preparation angles (15° and 30°).

6) The location of reflectors was poorly situated for high refracted angles ($\theta \geqslant 60^\circ$), due to curvature of the ultrasonic beam in the dendritic textures for long sound paths.
A refracted angle $\theta = 45^\circ$ is therefore the best suited direction to inspect the maximum volume of this weldment and gave the best conditions for detection and location of flaws.

This confirms the directions pointed out by the ultrasonic propagation study in the cylindrical samples (§ 3.2.1.4, Fig. 6).

4.2.2. Weldment (II).

1) Various areas of the joint possessed different ultrasonic propagation characteristics:
   - the ferritic steel is very permeable to ultrasonic waves;
   - the coarse grained texture of the austenitic cast stainless steel produced a drastic and non uniform attenuation in ultrasound, the S/N ratio being very small (some reflectors 65mm deep were not detected);
   - the dendritic textures as in 4.2.1.1).

2) As the parent materials were not symmetrical, the detection of the artificial flaws varied greatly with respect to direction:
   - when examining from the ferritic steel side, all the reflectors (except the notch n°. 9) are detected when $\theta = 45^\circ$;
   - when examining from cast stainless steel side, reflectors situated at a depth of 25mm were detected for $\theta \leqslant 60^\circ$, while the 55mm deep reflectors were no longer detected: the sound path in this steel must be reduced to detect the reflectors near the opposite surface.

3) The S/N ratio was very low for tests performed from the cast stainless steel side.

4) There were many structural spurious echoes at small refracted angles ($\theta \leqslant 30^\circ$) and also at angles close to weld preparation angles (10° and 20°).

5) The location of reflectors was poorly situated for small ($\theta \leqslant 10^\circ$) and high ($\theta \leqslant 60^\circ$) refracted angles owing to a long sound path in the dendritic textures of the buttering and the homogeneous weld.
   A $40^\circ \leqslant \theta \leqslant 45^\circ$ refracted angle is steel is therefore the best-suited direction to inspect the maximum volume of this weldment and provides the best conditions for flaw detection and location.
   This also confirms the directions pointed out by the ultrasonic propagation study in the cylindrical samples (§ 3.2.2.3, Fig. 7).

4.3. The effect of frequency.

A *Panametrics V115* (ϕ 0.75" – 10 MHz broadbard) transducer was connected to the Panametrics 5052 PR Pulser Receiver. 30mm (weldment I) or 25mm (wledment II) deep side drilled holes were examined with longitudinal waves at a 45° refracted angle in the steel.

The – 3 dB frequency spectrum bandpath for signals obtained from each reflector showed that 1.5 MHz was well suited for both weldments.

5. CONCLUSIONS.

The above results make it possible to define the characteristics of suitable probes: they should emit longitudinal waves at 1.5 MHz at an angle of 45° in steel.

At the present time, FRAMATOME is testing some special probes manufactured in both its own and in INSA'S Laboratories.

Other commercially available probes, specially manufactured for inspection of austenitic welds, will also be tested. The transducers giving the best results will be used for testing representative blocks with actual flaws.

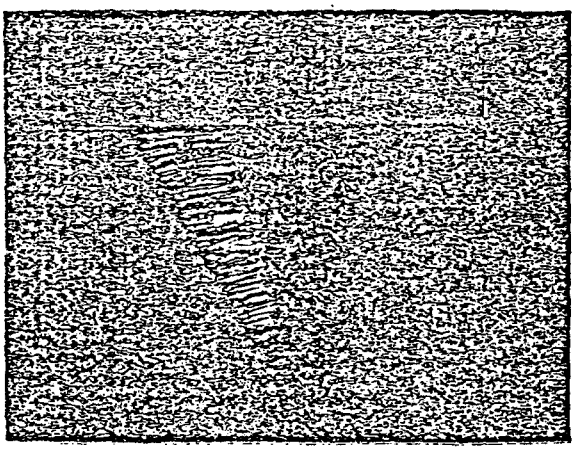

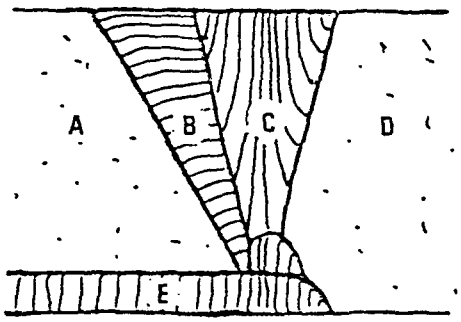

Macrograph

Area A:

Ferritic forged steel parent material.

X 100

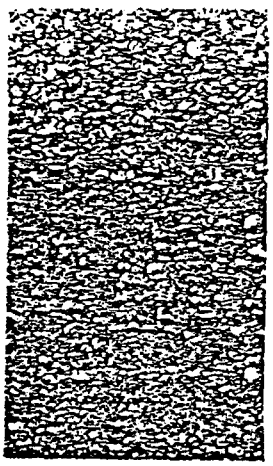

Area D:

Austenitic forged stainless steel parent material.

X 100

Area C:

Manual metal arc buttweld (austenitic steel).

Perpendicular to weldment skin.

X 100

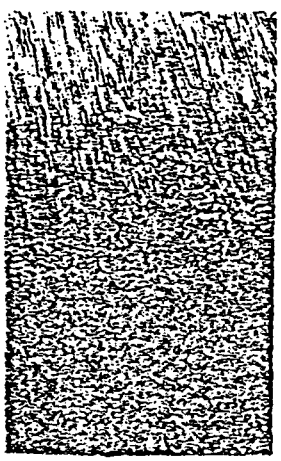

Area C

Manual metal arc buttweld (austenitic steel).

Parallel to the weldment skin.

X 100

Micrographs.

Fig. 1 — Weldment (I) — Metallography

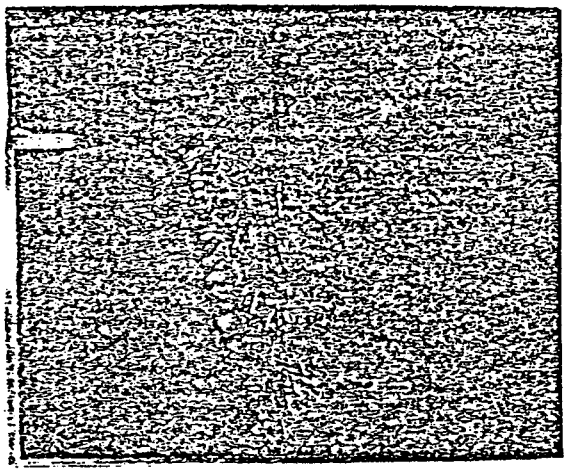

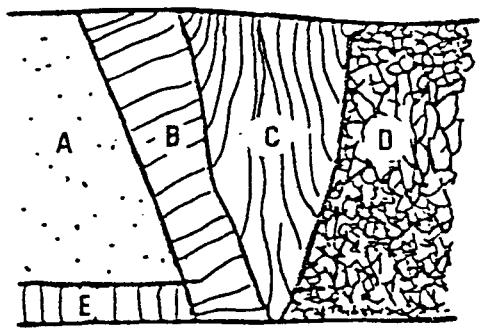

Macrograph

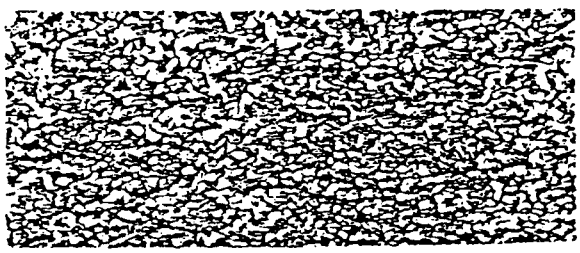

Area A:

Ferritic cast steel parent material.

X 100

Area D:

Austenoferritic cast stainless steel parent material.

X 100

Micrographs.

Fig. 2 – Weldment (II) – Metallography

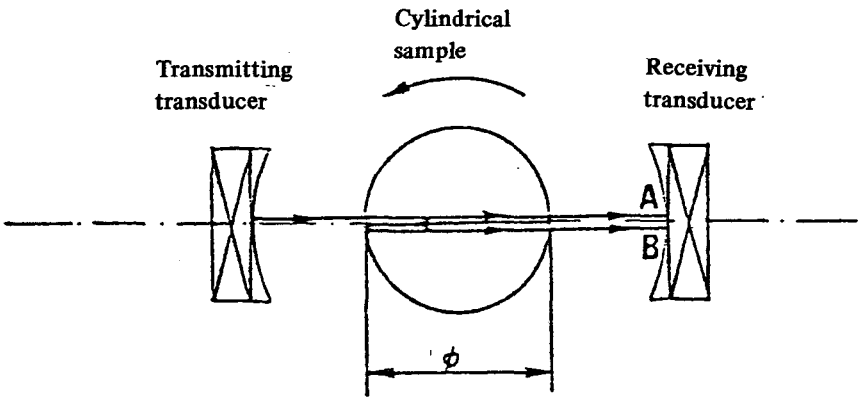

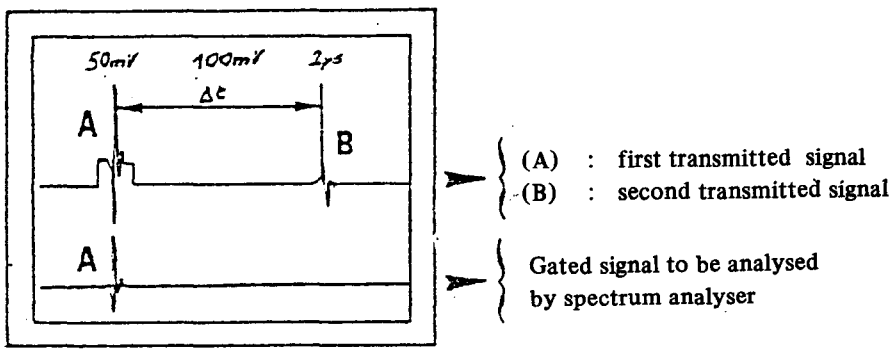

Screen display

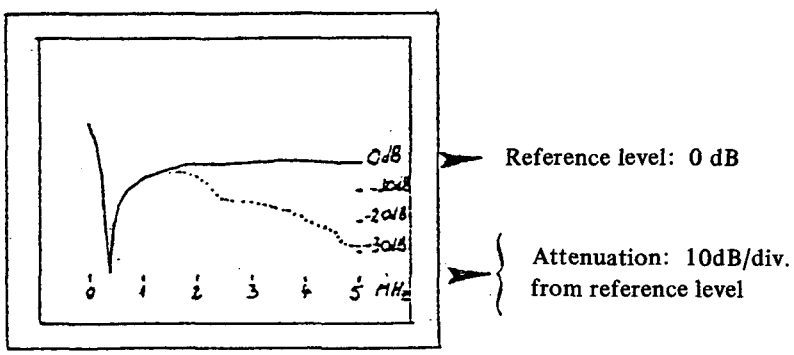

Frequency spectrum

longitudinal wave velocity in the cylindrical sample: $V = \frac{2\phi}{t}$

Fig. 3. Attenuation and velocity measurement methods.

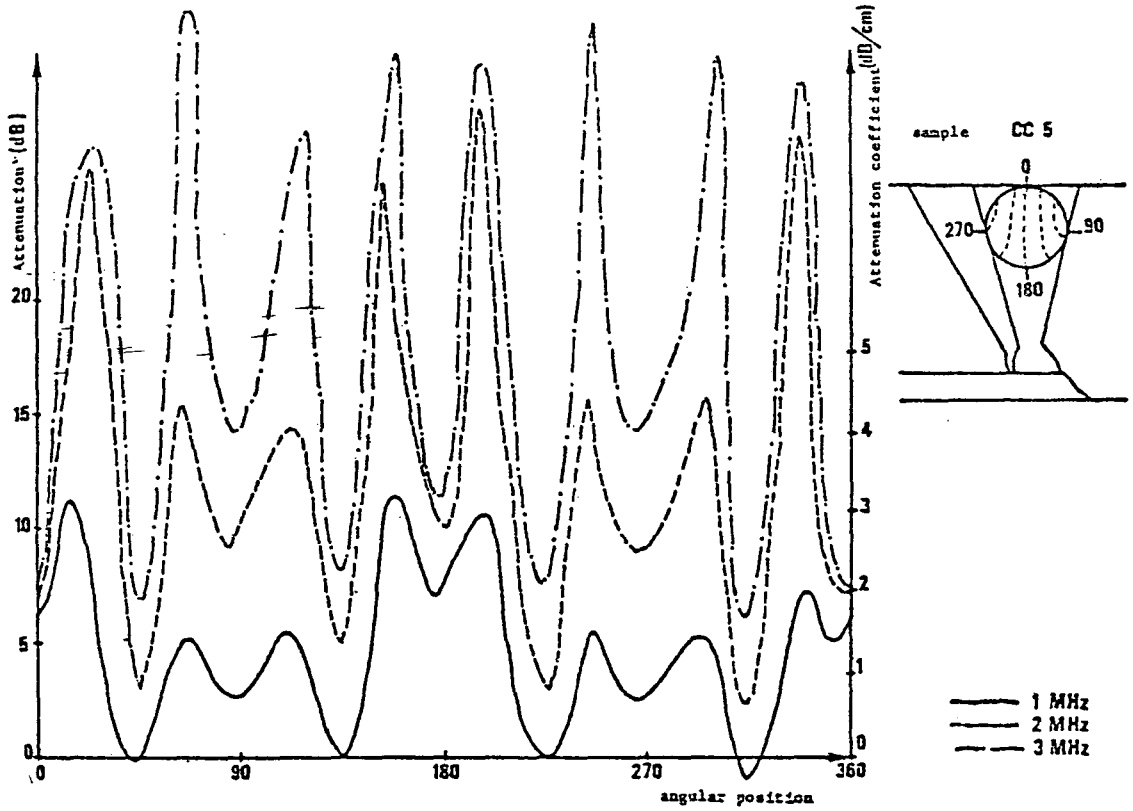

Fig. 4. Longitudinal wave attenuation in the manual metal arc buttweld Weld Weldment (I), area (C).

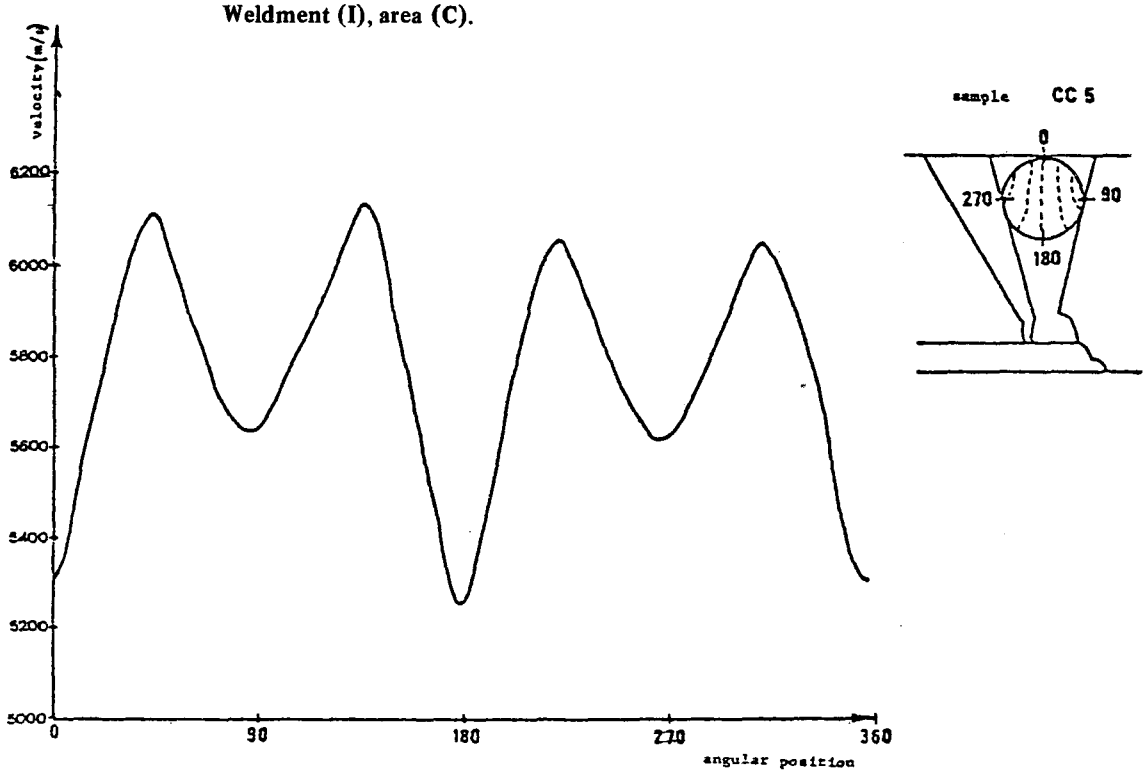

Fig. 5. Longitudinal wave velocity in the manual metal arc buttweld Weldment (I), area (C).

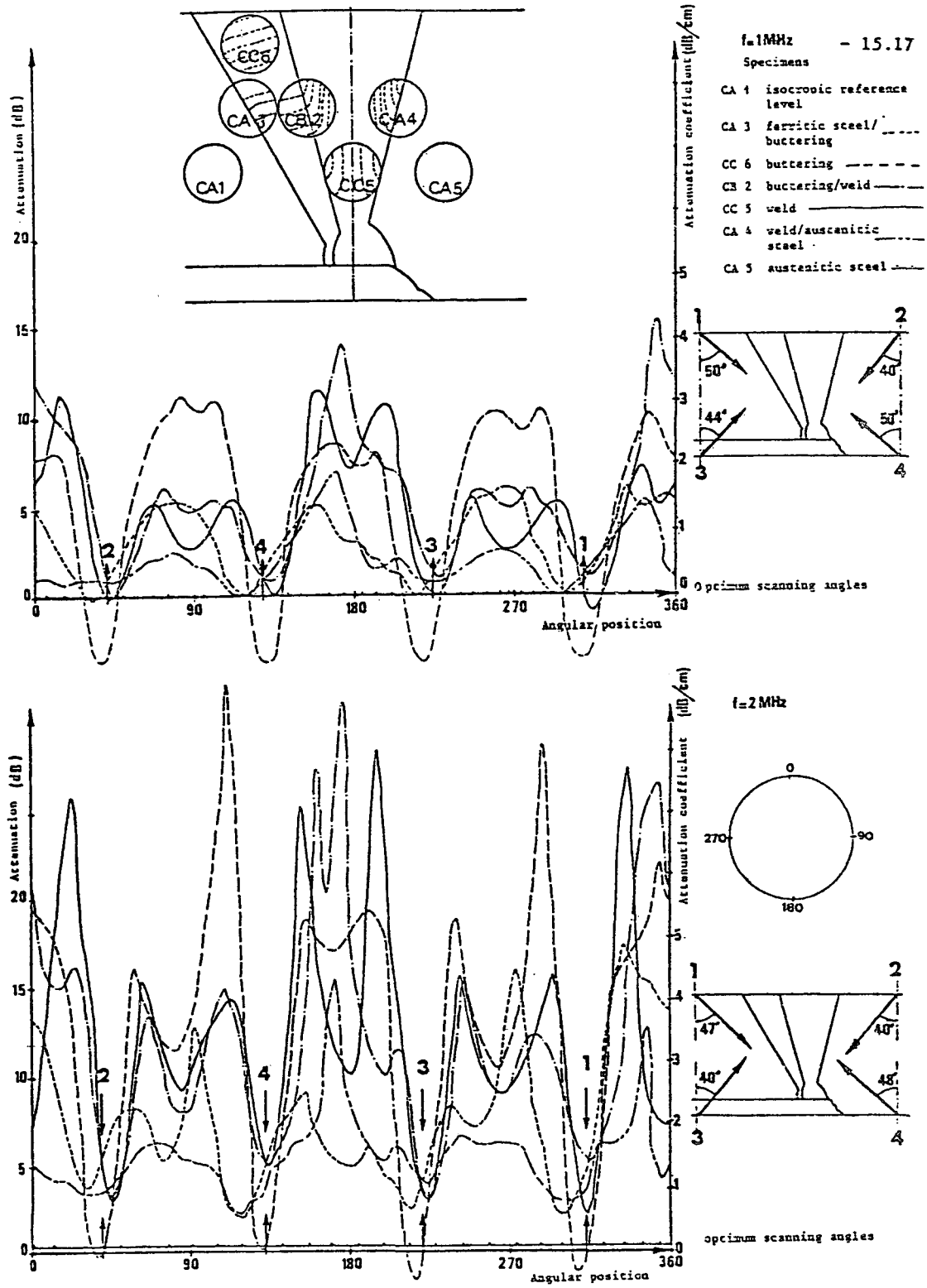

Fig. 6. Weldment (I) Attenuation in the various cylindrical samples at 1 and 2 MHz

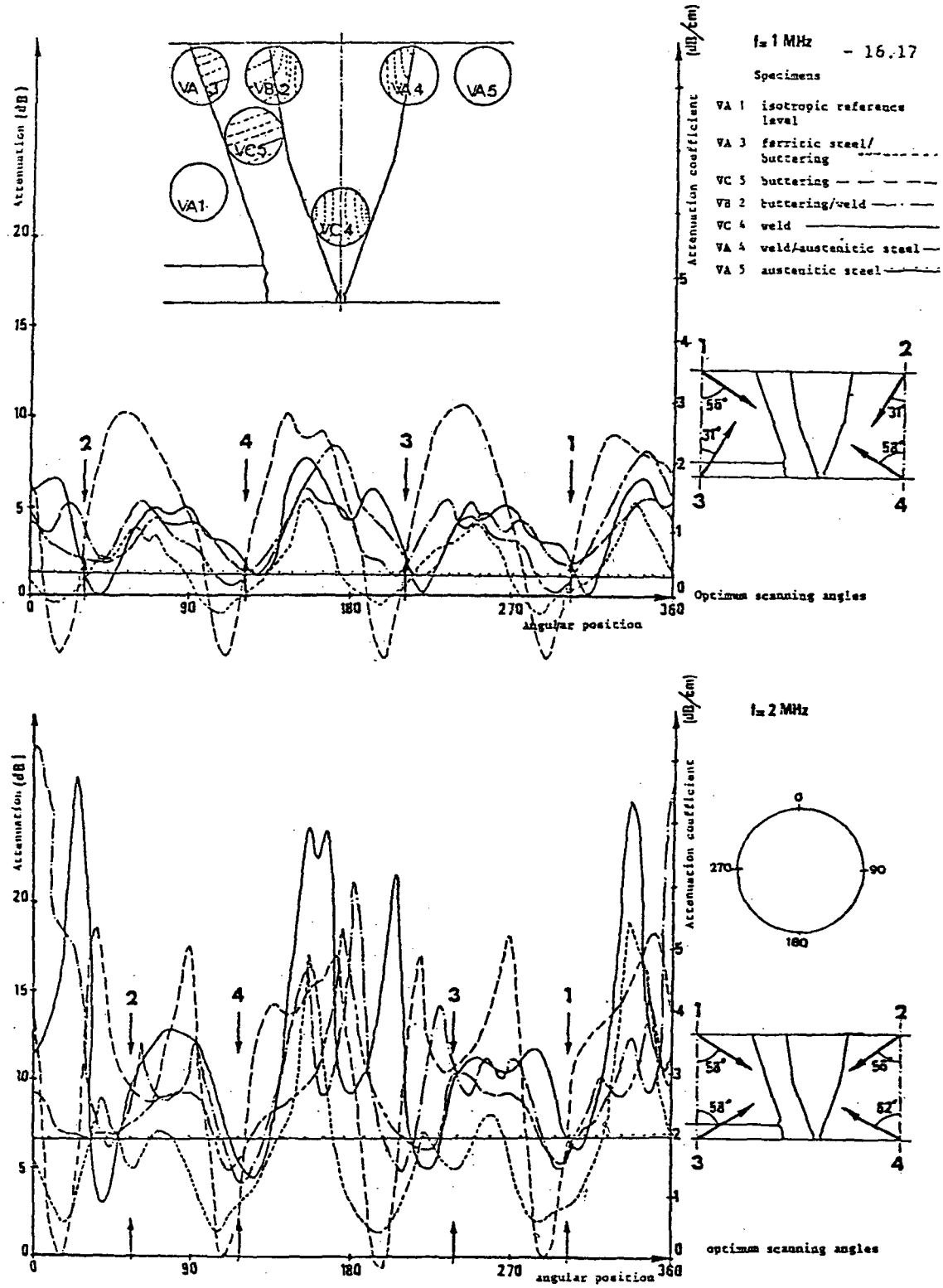

Fig. 7. Weldment (II) — Attenuation in the various cylindrical samples at 1 and 2 MHz.

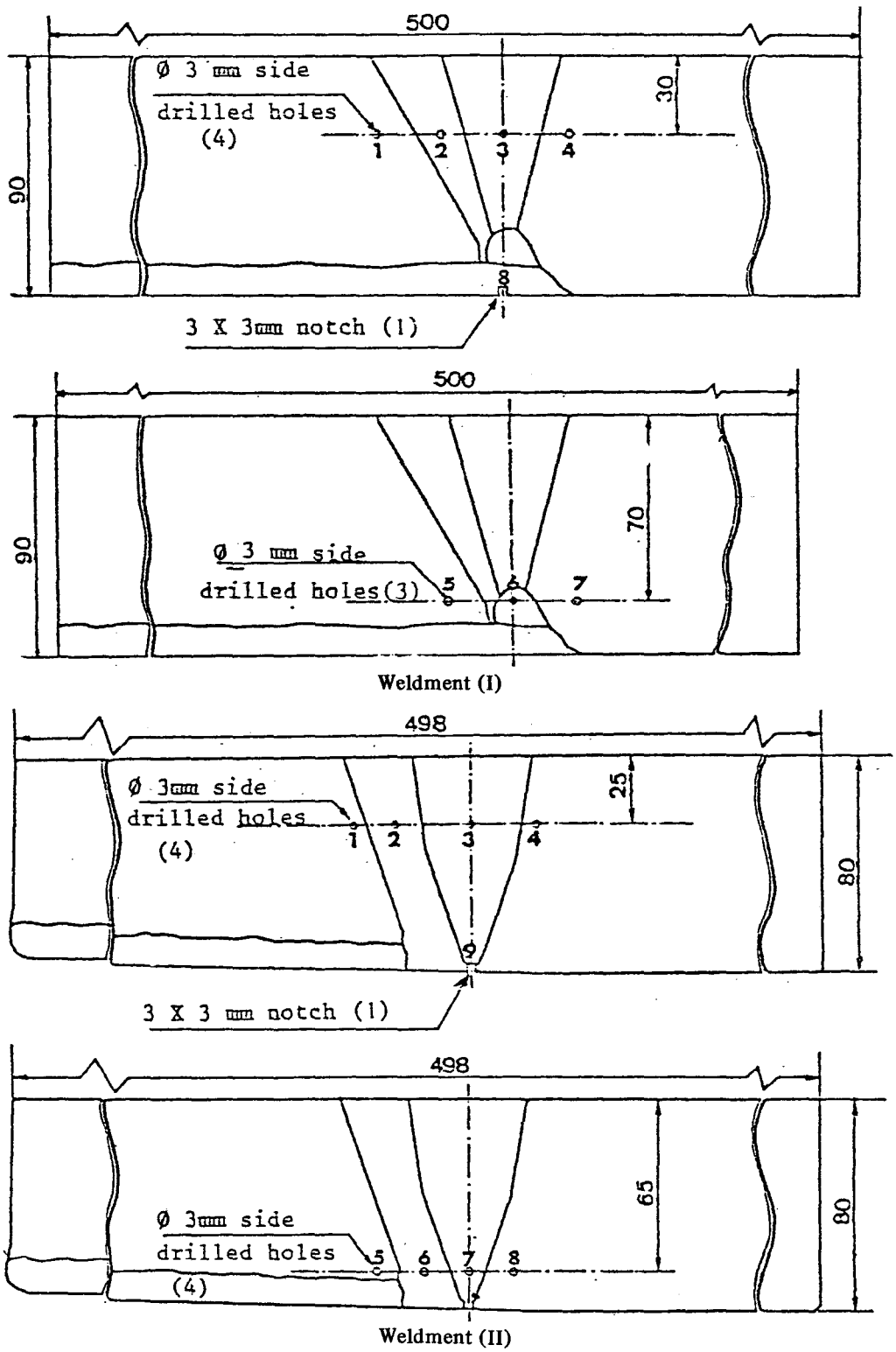

Fig. 8. Test-blocks with machined reflectors